

# Secure Information Embedding and Extraction in Forensic 3D Fingerprinting

Canran Wang\*, Jinwen Wang\*, Mi Zhou†, Vinh Pham†,  
Senyue Hao‡, Chao Zhou‡, Ning Zhang\*, and Netanel Raviv\*

\*Department of Computer Science and Engineering, Washington University in St. Louis

†Department of Electrical and Systems Engineering, Washington University in St. Louis

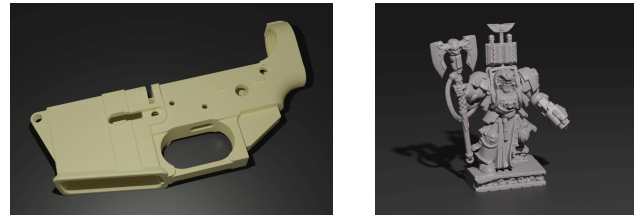
‡Department of Biomedical Engineering, Washington University in St. Louis

**Abstract**—The prevalence of 3D printing poses a significant risk to public safety, as any individual with internet access and a commodity printer is able to produce untraceable firearms, keys, counterfeit products, etc. To aid government authorities in combating these new security threats, several approaches have been taken to tag 3D-prints with identifying information. Known as a fingerprint, this information is written into the object using various bit embedding techniques; examples include varying the thickness of the molten thermoplastic layers, and depositing metallic powder with different magnetic properties. Yet, the practicality of these techniques in real-world forensic settings is hindered by the adversarial nature of this problem. That is, the 3D-printing process is out of reach of any law enforcement agencies; it is the adversary who controls all aspects of printing and possesses the printed object. To combat these threats, law enforcement agencies can regulate the manufacturing of 3D printers, on which they may enforce a fingerprinting scheme, and collect adversarially tampered remains (e.g., fragments of a broken 3D-printed firearm) during forensic investigation.

Therefore, it is important to devise fingerprinting techniques so that the fingerprint could be extracted even if printing is carried out by the adversary. To this end, we present SIDE (Secure Information Embedding and Extraction), a fingerprinting framework that tackles the adversarial nature of forensic fingerprinting in 3D prints by offering both secure information embedding and secure information extraction. First, with the help of ARM TrustZone, SIDE protects the integrity of the information embedding process such that the 3D-print is guaranteed to be tagged with the correct fingerprint. Second, by devising coding-theoretic techniques, SIDE is *break-resilient*, i.e., it allows correct fingerprint extraction even if the adversary breaks the 3D-print to at most a certain number of parts.

## 1. Introduction

3D printing brings about a revolution in consumption and distribution of goods. However, the prevalence of this technology exposes the public to various security threats. Any individual with a commercial 3D printer and internet access is able to produce untraceable firearms and counterfeits of IP-protected products (Figure 1) [1]–[4]. To aid authorities and law enforcement agencies in combat-



(a)

(b)

Figure 1: Renderings of (a) a 3D printed lower receiver of an AR-15 rifle. While US law regulates commercial distribution of this receiver, it can be easily manufactured privately using 3D printing technology, resulting in untraceable firearms known as *ghost guns*, and (b) an IP-protected tabletop wargame miniature that is illegally scanned with a 3D scanner.

ing these threats, fingerprinting 3D printed objects is one potential solution. In a fingerprinting scheme, a 3D-printer embeds uniquely traceable data into the printed object (e.g., timestamp, geolocation, printer ID, etc.), that can later be extracted to trace the perpetrator, e.g., if the object was confiscated or left at a crime scene.

Various techniques for embedding bits in 3D printed objects have been proposed in the literature. For instance, embedding tags on the surface of the object by varying layer thickness [5], altering layer material [6], inserting cavities inside the object [7], altering the surface of the object by varying printing speed [8], embedding RFID-tags [9]–[11] or QR codes [12], [13], inserting acoustic barcodes using surface bumps [14], etc. For a broad introduction to the topic see [15], [16]. An orthogonal line of work in the forensic 3D fingerprinting literature, which does not involve embedding nor extraction of bits, is based on identifying printers from their 3D-prints. This is done using machine-learning methods, based on manufacturing imperfections of printer components reflected on the print results [17].

The practicality of any such bit embedding technique, however, is hindered by a fundamental obstacle, i.e., *the adversary controls the printing*. First, the adversary has full control over the entire printing process. This gives the adversary the ability to manipulate information embedding, e.g., the adversary may bypass the information embedding

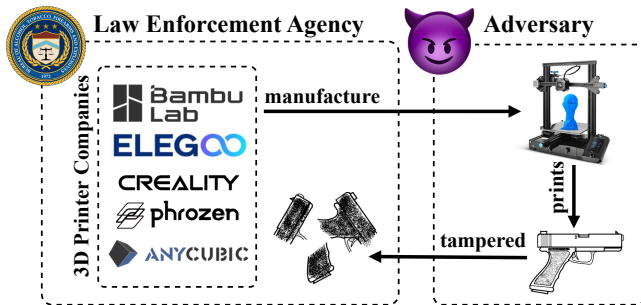


Figure 2: Law enforcement agencies only regulate 3D printer manufacturers, and confiscate adversarially tampered 3D-prints. The printing process and the printed object are fully controlled by the adversary, and are beyond the reach of law enforcement.

module installed on the printer and print a fingerprint-free firearm. Second, the adversary is in possession of the 3D prints, which may be broken after committing the crime, making the embedded information unrecoverable.

On the other hand, law enforcement agencies are restricted to merely regulate the manufacturing and distribution of commercial 3D printers. Once the printer is handed over to the (potential) adversary, the agencies can hardly monitor its usage, and can only attempt to recover information from adversarially tampered 3D-prints during forensic crime investigation (Figure 2).

Indeed, any embedded bits can be stripped-off from the 3D model file before printing, and any tag can be stripped-off using household items, as the printed object itself could be melted, deformed, or simply broken apart. As such, the aforementioned methods fail in the face of an adaptive adversary<sup>1</sup> that tampers with the printing process and the prints, since they rely on the integrity of both the information embedding process and the geometric shape of the printed object. Therefore, a practical fingerprinting scheme must overcome the following two key challenges under the circumstances in which both the printing and the prints are out of reach of law enforcement authorities.

*Challenge 1 (Embedding):* Guarantee *successful information embedding*, even in the face of an adaptive adversary that is fully aware of, and is able to interfere with, the embedding process.

*Challenge 2 (Extraction):* Guarantee *successful information extraction*, even in circumstances where the 3D-prints are adversarially tampered.

To this end, we design and implement SIDE, a Secure Information EmbedDing and EXtraction framework that is robust against an adaptive adversary that controls the printing process and may tamper with the printed object. Specifically, our contribution in this work is three-fold:

- *Secure information embedding:* We incorporate SIDE with a Trusted Execution Environment (TEE)

1. An *adaptive adversary* in a knowledgeable attacker that is fully aware of the information embedding/extracting scheme.

into the 3D printing process in order to protect its control-flow integrity. Consequently, the information embedding procedure is guaranteed to succeed even if the adversary is able to compromise the printer’s OS.

- *Secure information extraction:* We develop *break-resilient codes* (BRC), which are coding-theoretic techniques for information extraction from the 3D-prints, and incorporate them with SIDE. We develop corresponding decoding algorithms, and formally prove that they correctly extract the information even if the geometric shapes are adversarially broken to at most a certain number of parts; the maximum supported number of parts serves as a security parameter. As a result, the law enforcement agency is guaranteed to extract the information correctly.
- *Implementation:* We implemented and tested a prototype of SIDE. On the secure information embedding side, we realize SIDE on a Creality Ender 3 3D printer controlled by a Raspberry Pi 3B board, with OP-TEE V3.4 support enabled in its ARMv8-A architecture to protect the control-flow integrity of the printing process. On the secure information extraction side, we implemented efficient BRC encoder and decoder. The encoded information is embedded in the printed object by varying layer thickness, and is read by a Leica S9D microscope. In multiple experiments, we printed objects with embedded information, broke them apart, and managed to read out the embedded information successfully.

## 2. Background and Related Work

### 2.1. 3D Printing

3D Printing, commonly referred to as Additive Manufacturing (AM), has emerged as a revolutionary technology with profound implications across various industries. In contrast to the traditional *subtractive* manufacturing during which materials are consecutively removed from the work-piece, 3D printing refers to an *additive* process of creating a physical object and is typically done by laying down many thin layers of material in succession.

Numerous technologies have been developed for 3D printing. By and large, they differ by which material is in use and how layers are formed. A layer can either be formed by using a nozzle that deposits molten thermoplastics while shifting back and forth on a surface, e.g. Fused Deposition Modeling (FDM), by depositing a layer of liquid polymers and curing it by ultraviolet light exposure, e.g., Stereo lithography Appearance (SLA), or by depositing powdered material over the surface and binding it using high-energy laser beams, e.g., Selective Laser Sintering (SLS).

The manufacturing process starts with generating G-code commands from the user-input 3D model file. In detail, the slicer software operates by converting the model into discrete 2D diagrams, each represents a planar cross-section

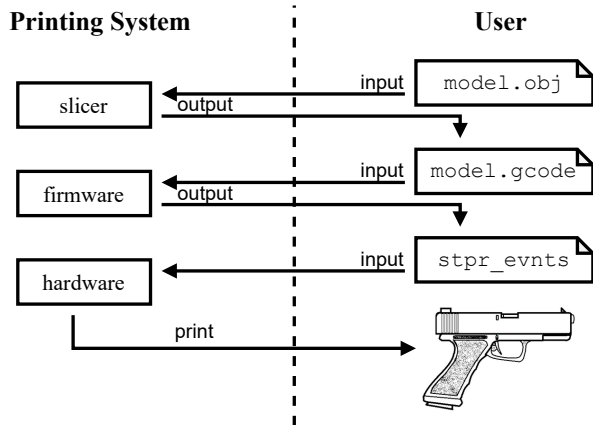


Figure 3: Illustration of the printing process. At first, the user feeds the 3D model `model.obj` to the slicer software and obtains `model.gcode`, which involves a series of commands for the printer. The printer firmware then translates these high-level commands to low-level stepping events and other hardware control instructions (`stpr_evnt`), which are then fed to the printer hardware for the physical printing process. To guarantee secure information embedding, a fingerprinting scheme must protect the control-flow integrity of this process.

of the model along the printing direction at a certain height. Then, the slicer creates a series of G-code commands to instruct the printer about how to produce the corresponding layers of the diagram sequence.

In this research, we focus on the FDM technology for its prevalence in commodity 3D printers (compared with SLS), as well as the profound mechanical strength offered to the printed objects (compared with SLA). As a result, the G-code commands for FDM printers may include the nozzle movement along the  $x$ ,  $y$ , and  $z$  axes, the extrusion of material, nozzle/bed temperature, and other specific aspects based on the printer’s capabilities.

A typical FDM printer involves four stepper motors, which are actuators that rotate in discrete angular steps of constant degree. Three of the motors control the nozzle movement in the Cartesian space, and one is responsible for filament extrusion. However, a G-code command specifies only the expected action of the printer hardware in a relatively high level, while the low-level implementation is not addressed. For example, the command

```
G1 X98.302 Y96.831 E15.796
```

merely instructs the printer to move its nozzle from its current position to location (98.302, 96.831) in the  $x$ - $y$  coordinate (with its position relative to the  $z$  axis unchanged), and simultaneously extrude 15.796 millimeter of molten thermoplastics. Completing this operation requires a series of stepping events, and each of them defines the exact timing and direction to trigger one of the four stepper motors for a single angular step.

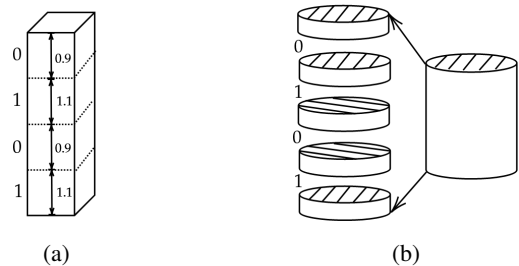


Figure 4: Two possible methods for embedding bits in a 3D printed object with little to no effect on functionality: (a) Embedding by layer thickness; thicker layers represent 1 and thinner layers represent 0. (b) Embedding bits using the orientation of adjacent layers; if two adjacent layers are oriented similarly, it is a 0, and if oriented differently, it is a 1. Both left and right figures contain the bits 0101.

To this end, the printer *firmware* plays a crucial role in bridging the G-code and printer hardware. In addition to commanding heaters and other applicable components, the firmware translates the G-code commands to a series of stepping events for the actuators, and the execution of them concludes the printing process. See Figure 3 for a complete illustration of the printing process.

It is worth noting that the translation task is non-trivial, and has a significant impact on print quality. For instance, a sudden jerk of the printer nozzle may lead to uneven deposition of print material, which jeopardizes the final print quality or even fails the print. In contrast, a nozzle movement with smooth velocity change is generally preferred. Therefore, the print quality may be significantly improved with an updated firmware, and the same G-code may be executed on printers with completely different builds.

## 2.2. Existing 3D Fingerprinting Methods

Several methods for embedding bits in 3D-printed objects have recently been proposed in the literature. These technologies allow the printer to vary either the orientation of the nozzle, the thickness of the layer, or the printing speed. Within reasonable bounds, varying either of those has a marginal effect on the functionality of the object. By varying layer thickness, for example, the printer can embed a 0 by printing a layer that is slightly thinner, and a 1 by printing a layer that is slightly thicker, than some reference thickness. By varying the orientation of the nozzle, bits can be embedded by the relative orientation of adjacent layers; for example, if two adjacent layers are oriented similarly, the embedded bit is 0, and otherwise it is 1. Both methods are illustrated in Figure 4.

Similar ideas have been implemented successfully in several recent works. Delmotte *et al.* vary the thickness of each layer across several adjacent layers to create a matrix of bits that is visible to the naked eye on the surface of the object [5]. Parity bits were then added to resolve reliability issues in some cases, and additional noise patterns were

discussed, such as orientation issues and sanding. In the method LayerCode [18], variations in color and thickness were used to embed a barcode on the surface of the printed object, that can be retrieved using a smartphone camera.

An orientation-based method has been implemented in [19], where the authors print a reference layer that is circularly grooved by a sequence with low auto-correlation. Data is embedded in all other layers by the respective angle of the layer to the reference layer; this enables encoding with alphabet size larger than two.

Various other creative ideas have been explored, including embedding information-carrying cavities within the object [20], [21], water-marking the 3D-mesh of the surface of the object [22], inserting RFID tags [9], inserting a series of notches which create an acoustic barcode when tapped [14], etc. In the data extraction phase, most existing methods rely on an RGB camera, a 3D scanner, or an ordinary scanner. Future technologies however, such as the ones in Figure 4, might require an industrial CT scanner.

However, we argue that none of these approaches is suitable for forensic applications. First, they all implicitly assume that a mechanism for correct information embedding is in place. Such a mechanism is crucial since in most scenarios the adversary owns the printer and/or the file, and might potentially remove the embedded bits altogether. Second, none of the methods is provably resilient to adversarial tampering; they can be easily breached by an adaptive adversary that can scrape the object or break it apart.

PrinTracker [17] represents a different line of works, which apply machine-learning based methods to identify the intrinsic fingerprint which results from printer hardware imperfections. The variations of printer components arising from manufacturing errors are essentially inevitable, and create perceivable differences between objects made from different 3D-printers, even if they are printed from the same 3D model. These differences form a unique printer fingerprint, and can be extracted from the printed objects with commodity scanners.

Unlike the aforementioned techniques, PrinTracker does not embed bits into the object; although it also considers the adversarial nature of forensic applications, as well as potential attacks, it is different from the information embedding solution proposed in our work. Further, it remains to be shown if the extraction, storage, and identification of such imperfections scales well to a large number of printers. Our proposed solution allows for embedding arbitrary bits, which enables a variety of forensic applications, including but not limited to fingerprinting. For example, certain applications may require the embedding of timestamp or geolocation of the printing into the printed object in order to check whether the printer has been misused in unauthorized time and location.

### 2.3. Trusted Execution Environment

Trusted Execution Environments (TEEs) have emerged as a solution to the problem of protecting sensitive and

critical operations in modern computing systems. With hardware and/or software isolation mechanisms, a TEE provides a secure execution space for the processes running within, which are commonly referred as *Trusted Applications* (TAs). The TAs, as well as their assets, cannot be accessed or tampered by unauthorized codes from the outside world, i.e., the main operating system which is commonly referred to as the Rich Execution Environment (REE) or *normal world*.

Hardware implementations of TEE include ARM TrustZone, Intel Software Guard Extensions (SGX), and RISC-V Keystone. Meanwhile, software development kits (SDKs) for TEE are also available [23], [24] for the ease of TA developments. Together, TEE have hosted applications across numerous domains, including access control [25]–[27], cloud computing [28]–[32], and real-time systems [33]–[35].

### 2.4. Coding Methods

Secure information extraction is essentially a problem of communicating in the presence of (potentially adversarial) noise. Such problems are studied in the information-theoretic literature under the title of coding theory [36]. A typical problem setup in coding theory includes a sender (e.g., the printer), which would like to send a message (e.g., printer ID) to a receiver (e.g., law-enforcement). This must be accomplished successfully even if an adversary (e.g., a criminal) injects adversarial noise that is limited by some security parameter.

Coding problems of information extraction from fragments have been previously studied in the literature, motivated by applications in DNA storage. In particular, several variations of the so-called *torn-paper channel* were studied in [37]–[41], where [37]–[39] focused on a probabilistic error model which is incompatible with our adversarial setting, and [40] studied an adversarial error model in which fragment are restricted in length. Most closely related, [41] studied *t*-break codes, which coincide with our problem definition (given shortly). They provided a theoretical analysis of the fundamental limits, and an (almost) matching code construction. However, the scheme described in [41] involves random encoding and is only effective for a very large number of embedded bits. Our work herein addresses the same model of [41], yet at a much simplified framework which can be easily employed in practical settings, albeit below the maximum theoretical information rate.

### 3. Threat Model

We consider an adaptive adversary, i.e., one who is fully aware of the proposed embedding/extracting scheme. The adversary wishes to commit a crime, but is unable to obtain a certain required instrument, say, fails to pass background checks when attempting to purchase a firearm, or has insufficient financial means. Hence, the adversary manufactures the instruments independently, by downloading a 3D model file from the internet and feeding it to a commercial grade 3D-printer bought from a local electronics retailer.

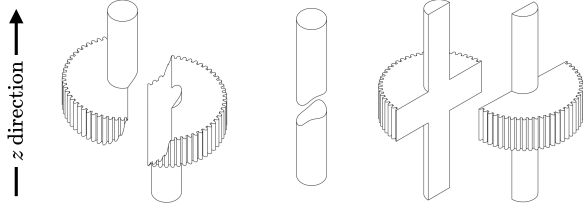


Figure 5: Possible types of break that cross multiple layers. In either case, the assembly of pieces may be inferred from their geometries.

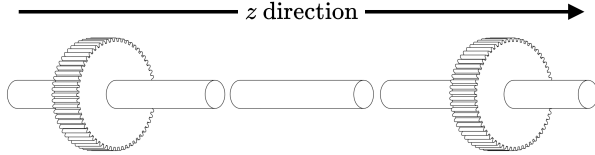


Figure 6: Fragments of a transmission shaft that is broken along the  $z$  direction. The correct assembly (i.e., order) cannot be inferred from their geometries.

We assume that the 3D printer does not require a background check to purchase. At the time of printing, the printer composes a binary string  $w$  to be embedded within the object. The content of such string may include a unique printer ID, the time and geolocation of the printing process, the identity of the file, etc, which aid the authorities to trace the perpetrator<sup>2</sup>.

The string  $w$  is embedded in every object printed by that printer using physical elements on the printing direction, e.g., altering layer thickness or material. We assume that the actuators (e.g., stepper motors) and other electronics (e.g., heater) of the 3D-printer are connected to a hardware platform (e.g., a control board) which supports a trusted execution environment (TEE). The TEE provides strong isolation on processor, memory, and peripherals. Specifically, the General-Purpose Input/Output (GPIO) port connecting to the printer hardware is driven by a secure program that resides inside the TEE, and the connection from the board to the hardware is also free of malicious tampering.

Meanwhile, the adversary is able to compromise the rich execution environment (REE) on the control board, including all necessary software components and the hosting operation system. Then, the adversary prints the object, commits the crime, and mechanically damages the printed tool, breaking it into pieces.

Breaks fall into one of two categories, depending on whether it crosses multiple layers or not. We intentionally disregard the former category of breaks, as it is likely to cause an irregular geometry of the broken section, which enables correct reassembly of the pieces. Moreover, the identical layer-thickness pattern of two matching fragments

2. In the upcoming implementations and experiments we focus solely on printer ID. The secure procurement and embedding of additional real-time identifying information is left for future studies.

provide enough hints to couple them together (See Figure 5 for illustrative examples).

Instead, we are particularly interested in the latter type of breaks, which occur along the printing direction and separate adjacent layers of the printed object. Our preference stems from the following observations.

- 1) 3D printers operate in a layer-by-layer fashion, and as a result, the printed objects have the lowest mechanical strength along the printing direction, making this type of breaks more frequent.
- 2) This type of breaks reveals limited information on the geometry of the tool that allows for reassembly (See Figure 6 for an illustrative example).

We assume that the pieces of the broken tool are confiscated by a law enforcement agency after the crime has been committed. The agency is able to reassemble breaks of the first category (Figure 5), but not of the second (Figure 6). This results in at most  $t + 1$  fragments caused by at most  $t$  breaks of the second category, whose correct reassembly is unknown, where  $t$  is a security parameter that reflects time constraints, access to instruments, or physical strength limitations. The parameter  $t$  is crucial for the analysis of the system, since it prevents the adversary from breaking the object into arbitrarily many fragments, thus eliminate all chances of extracting the fingerprint.

Having obtained these  $t + 1$  unordered fragments, the agency reads the embedded bits from the fragments by examining the bit-embedding physical elements on the printing direction. The reading mechanism requires the use of additional technology such as a smartphone camera, a microscope, or a computed tomography (CT) device, depending on the thickness of the layers, the complexity of the object, the outside finish of the object (e.g., coating), and the external damage done by the adversary (e.g., scraping).

Finally, we emphasize that we *do not* rely on correct reassembly of the  $t + 1$  unordered fragments of the object, and base our secure information extraction techniques solely on the information content of the fragments. That is, the decoder (i.e., law-enforcement) is given a collection of  $t + 1$  unordered fragments, which cannot be assembled based on their geometric shape, and needs to recover the information successfully. Recovery must be successful in all cases in which the adversary breaks the object apart at most  $t$  times, in arbitrary positions along the  $z$  direction.

## 4. Secure Information Embedding

### 4.1. Preliminary and overview

To provide secure embedding, one must protect the control-flow integrity of the printing process shown in Figure 3. That is, the printer hardware must receive the instructions generated by the firmware. Meanwhile, the firmware must receive the G-code generated by the slicer, with the desired information embedded within.

However, the integrity of this control flow can be easily jeopardized by an adversary with full control over the REE

of the printer control board. For example, this adversary may bypass the slicing process by feeding to the firmware a G-code file that was generated independently (i.e., not by the designated slicer), and does not contain the embedded information. Alternatively, the adversary may control the printer hardware using a modified firmware, in order to similarly alter the information embedding process.

To address the aforementioned issues, SIDE employs a Trusted Execution Environment (TEE) to protect the control-flow integrity of the printing process; such a design is motivated by the resemblance between 3D printing and the compilation process of a program (e.g., a C program). Indeed, similar to human-readable C code which must be converted to assembly/binary, the 3D models must be converted to G-code which the printer firmware can recognize.

Furthermore, both G-code and assembly code are commands for lower-level hardware, but both are oblivious to the inner workings of that hardware. For example, a CPU instruction to fetch memory data to a register does not specify how this operation is implemented in the integrated circuit (IC). Meanwhile, two ICs that support the same instruction set may have completely different circuit designs. Examples of jeopardizing the compilation process have been shown in [42]; with a deliberately crafted compiler, benign source code may be miscompiled to a malware. A similar attack has also been demonstrated in the recent backdoor implantation in the XZ Utils [43].

## 4.2. Embedding Framework

The SIDE embedding framework employs a *host* application that resides in the REE. It solely provides a frontend interface to the printer users, accepting 3D models and passing them to the backend, which wholly resides in TEE. The SIDE backend involves four major functional modules, namely *codec*, *layer-gen*, *toolpath-gen*, and *firmware*.

At first, the *codec* encodes the information  $w$  to a break-resilient codeword  $c$ ; the details of the encoding process will be given in Section 5. Next, the SIDE backend proceeds to the actual printing process. Recall that our embedding method relies on varying the thickness of layers. Specifically, it first segments the model into constant-length *height intervals* along the printing direction, and then associates the  $i$ -th height interval with the  $i$ -th bit in  $c$ . The value of  $c[i]$  determines the thickness of layers within the corresponding height interval (see Section 6.1 for details).

After picking up the model file from the host application, the following procedure is executed by the SIDE backend for every bit of  $c$  for secure information embedding. For every  $c[i]$ , *layer-gen* generates the cross-sectional diagrams of its associating layers. Next, *layer-gen* passes the diagrams to *toolpath-gen* along with their corresponding heights, i.e., their distances to the printer bed.

The *toolpath-gen* module then determines the nozzle toolpath from the received data, which is usually represented as a G-code file. Indeed, the G-code document for  $c[i]$  instructs the 3D printer on how to build the object within a certain height interval. Finally, the *firmware* module picks

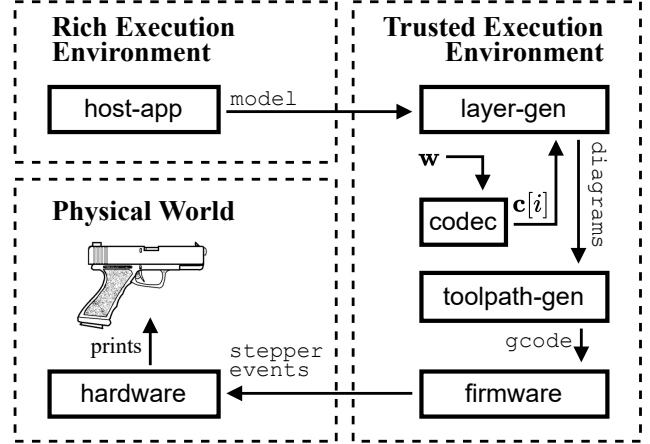


Figure 7: Illustration of the interactions among the rich execution environment (REE), the trusted execution environment (TEE), and the physical world during the printing process. At first, the 3D model is fed into the host application (in REE), which invokes *layer-gen* (in TEE) to perform slicing and information embedding. For every bit of the to-be-embedded codeword  $c$ , a G-code file is created by *toolpath-gen* and picked up by *firmware* (both in TEE). The *firmware* translates the G-code commands to stepper events, and invokes the hardware (stepper motors) to perform the actual printing in the physical world.

up the G-code document, and translates it to a series of stepper events. Through the board peripherals (GPIO), the SIDE backend passes these events to printer steppers, and conduct the actual printing in the physical world. This concludes the handling of  $c[i]$ , and a graphical illustration is shown in Figure 7.

Note that the above procedure is repeated for every bit of the BRC codeword  $c$ , and the printing process is concluded after handling all bits. Since the entire printing process is hidden in the trusted world and no intermediate data (e.g., a G-code file) is exposed to the user, the adversary is unable to strip off the embedded bits.

## 5. Secure Information Extraction

### 5.1. Preliminary and overview

The secure information extraction feature of SIDE is attributed to a *break-resilient code* (BRC), which is specifically developed for forensic fingerprinting purposes. Before being embedded, the to-be-embedded information  $w$  goes through an encoding process. The resulting codeword  $c$  has the *t-break-resilient property*; as the name suggests, the corresponding decoder is able to recover  $w$  even if the codeword is broken into at most  $(t+1)$  unordered fragments.

BRC includes an encoder which holds a binary string  $w \in \{0, 1\}^k$  (an information word, e.g., printer ID) for some integer  $k$ , that is to be encoded to a string  $c \in \{0, 1\}^n$  (a codeword). After encoding  $w$ , the codeword  $c$  is

embedded in a printed object. BRC may be applied to any possible bit embedding method, and yet in Section 6.1 we focus on varying layer thickness. For a security parameter  $t$ , an adversary breaks these  $n$  bits at arbitrary  $t$  locations or less, resulting in a multiset of at most  $t + 1$  fragments<sup>3</sup>.

**Example 1.** For a string  $\mathbf{c} = 0100011100$  and  $t = 3$ , the possible fragment multisets include

$$\{\{0, 0, 1000, 1110\}\} \text{ and } \{\{01000, 11100\}\}.$$

These bits are extracted from the fragments of the broken printed object, and then given to the decoder in an unordered fashion. The goal of the decoder is to reconstruct  $\mathbf{c}$  exactly in all possible cases, from which  $\mathbf{w}$  can be obtained, hereafter providing secure information extraction. The following notions from coding theory are employed as basic building blocks for BRC.

**5.1.1. Systematic Reed-Solomon Codes.** Systematic Reed-Solomon (RS) codes are a special type of Reed-Solomon codes, which have been widely employed in communication systems and data storage applications; for an introduction to the topic see [36, Ch. 5].

For integers  $k$  and  $n$  such that  $n > k > 0$ , a systematic  $[n, k]$  RS code is a set vectors of length  $n$  called codewords, each entry of which is taken from  $\mathbb{F}_q$ , a finite field with  $q$  elements. The first  $k$  entries of each codeword in a systematic RS code carry information in raw form, and the remaining  $n - k$  contain redundant field elements that are used for error correction. This code is *maximum distance separable* (MDS), a property which allows the recovering of a codeword, after being corrupted by  $a$  errors (incorrect symbols with unknown locations) and  $b$  erasures (incorrect symbols with known locations), as long as  $n - k \geq 2a + b$ .

Note that RS codes requires the finite field size  $q$  to be greater or equal to the length of the codeword, i.e.,  $q \geq n$ . Furthermore, we focus on the binary field and its extension field in this paper, in which  $q = 2^x$  for some integer  $x \geq 1$ , and any element can be represented by a binary string of length  $x$ .

**5.1.2. Run-length Limited Codes.** A run-length limited (RLL) code is a collection of codewords in which the length of runs of repeated bits is bounded. Specifically, in this paper we employ the RLL code from [44, Algorithm 1] for its simplicity of implementation.

**5.1.3. Mutually Uncorrelated Codes.** A mutually uncorrelated (MU) code has the property that for every two (possibly identical) codewords, the prefix of one is not identical to the suffix of another. As such, the codewords of a MU code do not overlap with each other when appearing as substrings of a binary string. MU codes has been extensively investigated in the past [44]–[53]. In this paper, we adopt a classic construction of MU code, in which each codeword starts with  $\lceil \log k \rceil$  zeros followed by a one, where  $k$  is the

3. For the flow of the paper, the proofs of theorems and lemmas are given in the appendix.

length of the (binary) information word. The last bit is fixed to one, and the remaining bits are free from zero runs of length  $\lceil \log k \rceil + 1$ .

**5.1.4. Distinct Block Codes.** Inspired by ideas from [44, Algorithm 1] and [54, Algorithm 1], we provide Alg. 3 that maps an input word to an array of distinct binary strings, and offer the inverse operation in Alg. 4. These procedures serve as an important component in BRC. Both algorithms, as well as proofs of their correctness, are given in the appendix.

## 5.2. Encoding

The encoding procedure of BRC takes a binary string  $\mathbf{w}$  as input and outputs a break-resilient codeword, and it is provided in Algorithm 1. At high level,  $\mathbf{w}$  will be converted to a sequence of shorter distinct binary strings with the method introduced in the previous section, and their order will be recorded and then protected using a Reed-Solomon code. Synchronization issues among the symbols of the Reed-Solomon code will be resolved using the RLL and MU techniques mentioned earlier.

In detail, let binary string  $\mathbf{w} \in \{0, 1\}^k$  be an information word, where

$$k = (l - t) \cdot m - 1,$$

and  $l$  and  $m$  are positive integers such that  $m \geq \lceil 2 \log l \rceil + 2$ . The encoding of  $\mathbf{w}$  begins by prepending it with  $\mathbf{p}^{(0)}, \mathbf{p}^{(1)}, \dots, \mathbf{p}^{(t-1)}$ , resulting in

$$\mathbf{u} = \mathbf{p}^{(0)} \circ \dots \circ \mathbf{p}^{(t-1)} \circ \mathbf{w} \in \{0, 1\}^{l \cdot m - 1}, \quad (1)$$

where  $\mathbf{p}^{(i)}$  is the binary representation of  $i \in [0, t - 1]$  in  $m$  bits (line 1). Then, as shown in line 2, the resulting string  $\mathbf{u}$  is fed into the function D-ENCODE (which is implemented in Algorithm 3) and mapped to an array of  $l$  pairwise distinct binary strings of length  $m$ , i.e.,

$$\text{dStrings} = (\mathbf{u}_0, \dots, \mathbf{u}_{l-1}). \quad (2)$$

Note that due to the implementation of D-ENCODE, the first  $t$  elements of  $\text{dStrings}$  remain intact, i.e.,  $\mathbf{u}_i = \mathbf{p}^{(i)}$  for all  $i < t$ , and they are referred as *markers*. In the next step, a key-value store  $\text{next}$  is defined to represent the *ordering* of elements in  $\text{dStrings}$  as follows (line 4–8). For every key  $\mathbf{s} \in \{0, 1\}^m$ , the value  $\text{next}[\mathbf{s}]$  is defined as

$$\text{next}[\mathbf{s}] = \begin{cases} \mathbf{u}_{i+1} & \text{if } \mathbf{s} = \mathbf{u}_i \text{ for } i \in [0, l - 2], \\ \mathbf{s} & \text{otherwise.} \end{cases}$$

Note that the value  $\text{next}(\mathbf{s})$  is well defined, since  $\mathbf{u}_i \neq \mathbf{u}_j$  for every  $i \neq j$  by the pairwise distinct property of  $\text{dStrings}$ . It is also worth noting that the mapping from  $\text{dStrings}$  to  $\text{next}$  is injective; one may recover  $\text{dStrings}$  from  $\text{next}$  by observing every key  $\mathbf{r}$  such that  $\text{next}(\mathbf{r}) \neq \mathbf{r}$ , and connecting every two  $\mathbf{r}_a, \mathbf{r}_b$  of them if  $\text{next}(\mathbf{r}_a) = \mathbf{r}_b$ .

We proceed to the treatment of  $\text{next}$ . Since the values in  $\text{next}$  are binary strings of length  $m + 1$ , they can be regarded as symbols in the finite field  $\mathbb{F}_{2^{m+1}}$ . They are sorted

---

**Algorithm 1** ENCODE (BRC encoding)

---

**Input:** An information word  $\mathbf{w} \in \{0, 1\}^k$ , where  $k = (l - t) \cdot m - 1$ , and  $l, m$  are positive integers such that  $m \geq \lceil 2 \log l \rceil + 2$ .

**Output:** A codeword  $\mathbf{c} \in \{0, 1\}^n$ , where  $n = l \cdot (m + \lceil \log m \rceil + 4) + t \cdot (4m + 11)$

- 1: Let  $\mathbf{u} \leftarrow \mathbf{p}^{(0)} \circ \dots \circ \mathbf{p}^{(t-1)} \circ \mathbf{w}$ , where  $\mathbf{p}^{(i)}$  is the binary representation of  $i \in [0, t - 1]$  in  $m$  bits.
- 2:  $\mathbf{dStrings} = (\mathbf{u}_1, \dots, \mathbf{u}_l) \leftarrow \text{D-ENCODE}(\mathbf{u})$
- 3: Let  $\text{next}$  be a key-value store with keys and values being element in  $\{0, 1\}^m$ .
- 4: **for all** keys  $\mathbf{s}$  in  $\text{next}$  in ascending order **do**
- 5:     **if** there exist  $i \in [0, l - 2]$  such that  $\mathbf{s} = \mathbf{u}_i$  **then**
- 6:          $\text{next}[\mathbf{s}] \leftarrow \mathbf{u}_{i+1}$
- 7:     **else**
- 8:          $\text{next}[\mathbf{s}] \leftarrow \mathbf{s}$
- 9:  $\mathbf{r}_1, \dots, \mathbf{r}_{4t} \leftarrow \text{RS-ENCODE}(\text{next}[\mathbf{s}_0], \dots, \text{next}[\mathbf{s}_{2m-1}], 4t)$ , where  $\mathbf{s}_i = \mathbf{p}^{(i)}$ .
- 10:  $\mathbf{c} = \text{MU}(\mathbf{u}_0) \circ \text{RLL}(\mathbf{d}_0) \circ \dots \circ \text{MU}(\mathbf{u}_{t-1}) \circ \text{RLL}(\mathbf{d}_{t-1}) \circ \text{MU}(\mathbf{u}_t) \circ \dots \circ \text{MU}(\mathbf{u}_{l-1})$ .
- 11: **Output**  $\mathbf{c}$

---

by their corresponding keys and fed into a systematic Reed-Solomon encoder, which then generates  $4t$  redundancy strings  $\mathbf{r}_1, \dots, \mathbf{r}_t \in \{0, 1\}^{m+1}$  (line 9). Note that such encoding is feasible since the codeword length  $2^m + 4t$  is smaller than the number of elements in  $\mathbb{F}_{2^{m+1}}$ .

The codeword  $\mathbf{c}$  consists of two parts. The first region is called the *information region*, as it is generated from  $\mathbf{u}_0, \dots, \mathbf{u}_{l-1}$ , which directly originate from the information word  $\mathbf{w}$ . The second region is called the *redundancy region*. As the name suggests, it is made from the redundant bits generated from  $\text{next}$ .

Define an encoding function  $\text{MU}$  which maps  $\mathbf{u}_i \in \{0, 1\}^m$  to a codeword  $\text{MU}(\mathbf{u}_i) \in \{0, 1\}^{m + \lceil \log m \rceil + 4}$  of a mutually-uncorrelated code  $\mathcal{C}_{\text{MU}}$ . The information region is hereby defined as

$$\text{MU}(\mathbf{u}_t) \circ \dots \circ \text{MU}(\mathbf{u}_{l-1}).$$

For  $i \in [0, t - 1]$ , define the  $i$ -th redundancy packet

$$\mathbf{d}_i = \mathbf{r}_{4i} \circ \mathbf{r}_{4i+1} \circ \mathbf{r}_{4i+2} \circ \mathbf{r}_{4i+3}$$

as the concatenation of four redundancy strings. Then, define an encoding function  $\text{RLL}$  which maps  $\mathbf{d}_i$  to a binary sequence  $\text{RLL}(\mathbf{d}_i) \in \{0, 1\}^{4m+11}$  that is free of zero runs of length  $\lceil \log m \rceil + 1$  or more, and introduces 7 bits of redundancy. The encoding  $\text{RLL}$  gives rise to the following lemma which is easy to prove.

**Lemma 1.** For every  $i \in [t]$ ,  $\text{RLL}(\mathbf{d}_i)$  does not contain any codeword of  $\mathcal{C}_{\text{MU}}$ .

The redundancy region is hereby defined as

$$\text{MU}(\mathbf{u}_0) \circ \text{RLL}(\mathbf{d}_0) \circ \dots \circ \text{MU}(\mathbf{u}_{t-1}) \circ \text{RLL}(\mathbf{d}_{t-1}).$$

Finally, the codeword  $\mathbf{c}$  is the two regions combined (line 10).

$$\begin{aligned} \mathbf{c} = & \text{MU}(\mathbf{u}_0) \circ \text{RLL}(\mathbf{d}_0) \circ \dots \circ \text{MU}(\mathbf{u}_{t-1}) \circ \text{RLL}(\mathbf{d}_{t-1}) \\ & \circ \text{MU}(\mathbf{u}_t) \circ \dots \circ \text{MU}(\mathbf{u}_{l-1}). \end{aligned}$$

### 5.3. Decoding

Algorithm 2 provides a procedure for extracting the information word  $\mathbf{w}$  from at most  $t + 1$  fragments of the respective codeword  $\mathbf{c}$ . The crux of this decoding procedure is to reconstruct the key-value store  $\text{next}$  (see Section 5.2), and based on which the information word  $\mathbf{w}$  can be obtained. Specifically, the decoding algorithm creates a key-value store  $\text{approxNext}$ , which is slightly different from  $\text{next}$ , using the information which appears in the fragments. Alongside the correctly identified redundancy strings,  $\text{approxNext}$  goes through a Reed-Solomon decoding process and is corrected to  $\text{next}$ . Having the correct  $\text{next}$  in hand, the correct  $\mathbf{dStrings}$  (Eq. (2)) can be found as described earlier. Then,  $\mathbf{dStrings}$  is fed into  $\text{D-DECODE}$  (Alg. 4), which is the inverse process of  $\text{D-ENCODE}$  (Alg. 3) to produce  $\mathbf{u}$  (Eq. (1)), whose suffix is the information word  $\mathbf{w}$ .

The decoding starts by distinguishing and decoding the discernible codewords of  $\mathcal{C}_{\text{MU}}$  from the fragments. Let  $\text{MU}(\mathbf{u}_i)$  be a discernible codeword in  $\mathcal{C}_{\text{MU}}$  which fully reside within one fragment, where  $\mathbf{u}_i$  is its respective decoding. If  $\mathbf{u}_i = \mathbf{p}^{(i)}$  for some integer  $i < t$ , it means that  $\mathbf{u}_i$  is a marker, and then the  $(4m + 11)$  bits after it is a redundancy packet (line 2). As such, the decoder passes the  $(4m + 11)$  bits after (if residing in the fragment) to an  $\text{RLL-decoder}$  and obtains four redundancy strings  $\mathbf{r}_{4i}, \mathbf{r}_{4i+1}, \mathbf{r}_{4i+2}, \mathbf{r}_{4i+3}$  (line 3–4). The process stops once no more such codewords can be found, and we have the following lemma.

**Lemma 2.** Let  $t_2$  be the number of breaks that fall in the redundancy region of the codeword. Then, the decoding algorithm is guaranteed to obtain  $4(t - t_2)$  redundancy strings.

*Proof.* The decoding algorithm may fail to obtain a redundancy packet due to the occurrence of a cut either in the packet itself, or in the preceding marker. Therefore, it is guaranteed to obtain  $t - t_2$  redundancy packets, and hence  $4(t - t_2)$  redundancy strings.  $\square$



---

**Algorithm 2** DECODE (BRC decoding)

---

**Input:** A multiset FRAGMENTS of at most  $t + 1$  (unordered) fragments of a codeword  $\mathbf{c} \in \mathcal{C}$ .

**Output:** The information word  $\mathbf{w}$  such that Algorithm 1 with input  $\mathbf{w}$  yields  $\mathbf{c}$ .

```
1: Let  $\mathbf{r}_i \leftarrow \text{empty}$  for all  $i \in [0, 4t - 1]$ .
2: for all codeword  $\text{MU}(\mathbf{u}_i) \in \mathcal{C}_{\text{MU}}$  in the fragments in FRAGMENTS and  $\mathbf{u}_i = \mathbf{p}^{(i)}$  for some integer  $i < t$  do
3:   Let  $\mathbf{m}_i$  be the  $4m + 11$  bits after  $\text{MU}(\mathbf{u}_i)$ , and  $\mathbf{d}_i \leftarrow \text{DE-RLL}(\mathbf{m}_i)$ .
4:    $\mathbf{r}_{4i} \leftarrow \mathbf{d}_i[0, m], \mathbf{r}_{4i+1} \leftarrow \mathbf{d}_i[m + 1, 2m + 1], \mathbf{r}_{4i+2} \leftarrow \mathbf{d}_i[2m + 2, 3m + 2], \mathbf{r}_{4i+3} \leftarrow \mathbf{d}_i[3m + 3, 4m + 3]$ 
5: Let approxNext be a key-value store such that approxNext[s] = s for all  $\mathbf{s} \in \{0, 1\}^m$ .
6: for all fragment  $\mathbf{f} = \mathbf{f}_{\text{start}} \circ \text{MU}(\mathbf{u}_a) \circ \dots \circ \text{MU}(\mathbf{u}_{a+s}) \circ \mathbf{f}_{\text{end}} \in \text{FRAGMENTS}$  do
7:   for all  $r \in [s - 1]$  do approxNext[u_{a+r}] = u_{a+r+1}.
8: next  $\leftarrow$  RS-DECODE(approxNext,  $\mathbf{d}_1, \dots, \mathbf{d}_{4t}$ )
9: Let dStrings =  $(\mathbf{u}_1, \dots, \mathbf{u}_t)$  be an array of such that next(u_i) = u_{i+1}.
10:  $\mathbf{u} \leftarrow$  DJ-DECODE(dStrings)
11: return  $\mathbf{u}[t \cdot m : ]$ 
```

---

The other discernible codewords of  $\mathcal{C}_{\text{MU}}$ , i.e., those encoded from non-markers ( $\mathbf{u}_i$ 's for  $i \geq t$ ), are used to construct a key-value store `approxNext`. Initially, `approxNext(s) = s` for every key  $\mathbf{s} \in \{0, 1\}^m$  (line 5). For each fragment  $\mathbf{f}$ , let

$$\mathbf{f} = \mathbf{f}_{\text{start}} \circ \text{MU}(\mathbf{u}_a) \circ \dots \circ \text{MU}(\mathbf{u}_{a+b}) \circ \mathbf{f}_{\text{end}},$$

where  $\mathbf{f}_{\text{start}}$  and  $\mathbf{f}_{\text{end}}$  are (possibly empty) prefix and suffix of  $\mathbf{f}$  with no discernible codeword from  $\mathcal{C}_{\text{MU}}$  that is encoded from a non-marker.

Then, in line 7, the decoder updates

$$\text{approxNext}[\mathbf{u}_{a+c}] = \mathbf{u}_{a+c+1},$$

for every  $c \in [b - 1]$ . Note that `approxNext` is identical to `next` up to a bounded number of errors.

**Lemma 3.** Let  $t_1$  be the number of breaks that occur in the information region of the codeword. Then, `approxNext` differs from `next` at no more than  $2t_1$  positions.

*Proof.* The decoding algorithm may fail to find a non-marker (i.e.,  $\mathbf{u}_i$  for  $i \geq t$ ) in the information region if a break occurs inside it. Hence, the algorithm fails to identify at most  $t_1$  non-markers. Notice that, failing to capture a non-marker  $\mathbf{u}_a$  affects at most two key-value pairs of `next`, i.e., `next[u_{a-1}]` and `next[u_a]`, and hence `next` and `approxNext` differ in at most  $2t_1$  positions.  $\square$

The decoding algorithm proceeds to correct the constructed key-value store `approxNext` to `next`, i.e., the key-value store generated in Algorithm 1 from  $\mathbf{w}$ , using the collected redundancy strings and a standard Reed-Solomon decoder (line 8). Note that the missing redundancy strings are erasures (line 1), since their locations are known. The success of the decoding process is guaranteed in the following theorem.

**Theorem 1.** Alg. 2, line 8 outputs the correct key-value store `next`.

*Proof.* Notice that in line 8, a codeword is constructed by coalescing the elements in `next` with redundancy strings  $\mathbf{r}_0, \dots, \mathbf{r}_{t-1}$ , and fed into a Reed-Solomon decoder. By

Lemma 2, the decoder obtains at least  $4(t - t_2)$  redundancy strings, and as a result, the constructed codeword contains less than  $4t_2$  erasures.

Meanwhile, Lemma 3 implies that the number of key-value pairs in which `next` and `approxNext` differ is bounded by  $2t_1$ . Hence, the systematic part of the constructed codeword has at most  $2t_1$  errors. Recall that the encoding process generated  $4t$  redundancy strings (symbols in  $\mathbb{F}_2^{m+1}$ ), and as a result, the decoding in line 8 is guaranteed to be successful since

$$2t_1 \cdot 2 + 4 \cdot t_2 \leq 4(t_1 + t_2) \leq 4t,$$

where the last transition follows since the actual number of breaks  $t_1 + t_2$  is at most the security parameter  $t$ . The proof is concluded since a  $(2^m + 4t, 2^m)$  Reed-Solomon code can simultaneously correct  $a$  errors and  $b$  erasures as long as  $2a + b \leq 4t$ .  $\square$

Next, the array `dStrings` is obtained from `next` (line 9), and the function D-DECODE (which is implemented in Algorithm 4 in the appendix) is employed to recover  $\mathbf{u}$ . Recall that  $\mathbf{u} = \mathbf{p}^{(0)} \circ \dots \circ \mathbf{p}^{(t-1)} \circ \mathbf{w}$ , and hence the decoding procedure concludes by returning the  $l \cdot m$  rightmost bits of  $\mathbf{u}$  (line 11).

Finally, the decoding procedure implicitly implies that the break-resilient code is also *lost-resilient* up to a certain threshold, shown as follows.

**Corollary 1.** The break-resilient code tolerates the loss of fragments that are shorter than  $2m + 2\lceil \log m \rceil + 8$  bits.

*Proof.* Alg. 2 does not use any fragments that is shorter than twice of the length of a codeword in  $\mathcal{C}_{\text{MU}}$ , which equals to  $2m + 2\lceil \log m \rceil + 8$ .  $\square$

## 6. Implementation

We implemented a prototype of SIDE and conducted experiments to validate its applicability.

## 6.1. Secure Information Embedding

In prototyping our design shown in Figure 7, we employ a Creality Ender 3 3D printer (Figure 10a), and a Raspberry Pi 3B board (with OP-TEE V3.4 support enabled in its ARMv8-A architecture, and Raspbian Linux 4.14.98-v7 installed for the normal world) to serve as the control board. We adopt a bit embedding method by varying layer thickness, with a slight modification to the methods presented in Section 2.2<sup>4</sup>.

As shown in Figure 8, every bit in the codeword corresponds to an interval of 0.36 millimeters along the printing direction. If value of the bit is 0, then the corresponding interval consists of three layers of 0.12 millimeters. Otherwise, the corresponding interval consists of two layers of 0.18 millimeters. These values are chosen to maximize information density, i.e., the number of bits that can be embedded per unit length, with respect to the minimum layer thickness (0.12 millimeters) offered by the Ender 3 printer used in the experiments.

The choice of this embedding method is based on the argument that any practical bit embedding method should satisfy the following three properties.

- 1) **Readability:** The embedded information is readable within reasonable costs.
- 2) **Robustness:** The embedded information cannot be easily destroyed.
- 3) **Obliviousness:** The embedding method is oblivious to both the information bits and the geometry of the printed object.

The readability requirement implies economical reading of bits from the broken object with respect to a given use case, which will be illustrated in the next section. The robustness requirement states that the embedded information must be sufficiently robust against adversarial tampering, within a certain bound. For example, the surface of the printed object may be easily abraded and as a result, embedding information on the surface is not robust. We note that layer thickness is an intrinsic property of the printed object, and cannot be easily altered, nor it is affected by breaking or scraping the object.

The obliviousness requirement decouples the embedding method both from the information to be embedded and from the 3D models. Examples which violate the obliviousness requirement include representing 1's by thick layers and representing 0's by thin layers; this will cause codewords with different number of 1's to have embeddings of different lengths. Moreover, embedding bits by altering the geometry of the printed object is also considered inappropriate, as it may significantly affect its functionality. Note that for any embedding method, imposing some requirement on the dimension of the 3D model is inevitable (e.g., that its size is sufficient for embedding a certain number of bits), and

4. Our proposed framework are not inherently restricted to any particular TEE implementation, printer model, and bit embedding technique, as long as those bits are manifested as physical elements on the printing direction. The choices are made for the sake of experiments.

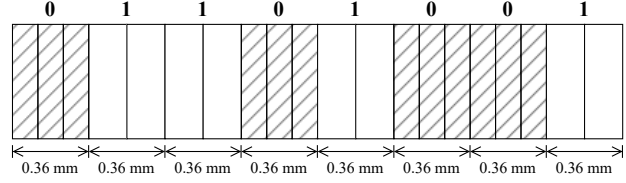


Figure 8: Demonstration of embedding 01101001 by varying layer thickness, in which each 0 is represented by three layers of 0.12 millimeters, and each 1 is represented by two layers of 0.18 millimeters. The length required for embedding one bit is irrelevant to its value.

we do not consider this as a violation of the obliviousness requirement. In our embedding method, as the thickness of layers add up to 0.36 millimeters in embedding either 0 or 1, the situation of height discrepancy is avoided, and the obliviousness requirement is satisfied. An example of printed objects with an embedded codeword is shown in Figure 9a.

Our development is heavily based on the Klipper open-source project [55] and t43 [56]. The former is a 3D printer firmware known for offering high precision stepper movements with supports to printers with multiple micro-controllers, and is suitable for running on low-cost devices such as Raspberry Pi. The latter is an open-source slicer program with basic functionalities and is purely written in C, making it suitable for trusted environments with restricted memory space and limited language support.

Our implementation follows the design shown in Figure 7. It involves a *host-app* that runs in the normal world, and four functional modules (*codec*, *layer-gen*, *toolpath-gen*, and *firmware*) that runs in ARM TrustZone. It is worth noting that the printing process involves looping through every bit of the codeword  $c$ . During each repetition, the corresponding layers of the bit are sliced and a G-code file is generated accordingly. This design avoids the potentially overlarge intermediate data (e.g., G-code of the entire model) that may exhaust the limited memory space of ARM TrustZone.

The *host-app* provides an interface for the printer users. It is developed on top of the Klipper command line interface, and allows users to configure the connected printer and submit 3D model files for printing. Written in Python, the host bridges the normal world with the trusted world using C Foreign Function Interface (CFFI).

The *codec* implements Algorithm 1 in C. It takes the to-be-embedded information  $w$  and outputs a break-resilient codeword  $c$ . The *codec* is a necessary component of the SIDE backend in the case where  $w$  is unknown at the manufacturing of the 3D printer, e.g., geolocation of the printing. Otherwise, the codeword may be simply generated in advance and hardcoded in the printer.

The *layer-gen* is developed on top of t43 and performs segmentation of the model file. In contrast to a normal slicer program that segments a 3D model altogether, *layer-gen* is called repeatedly during the examination of bits of



Figure 9: (a) A cuboid with an embedded BRC codeword. The codeword creates grooves on the outside of the object that are visible to the naked eye. For simplicity, we read the codeword using a microscope which detects light reflected from the top of each layer (Fig. 11). In cases where the outside grooves are not visible (e.g., scraping, filing, or coating), one can use a CT scanner to detect layer thickness. (b) A cuboid broken by hand to 3 fragments. Indeed, breaks occur naturally along cross-sections of the printing axis.

the codeword  $c$ . During each repetition, the `layer-gen` first determines the heights of the next two (or three) layers from the value of the current bit of  $c$ . For each layer, the `layer-gen` creates a diagram representing the cross section image of the model. The diagram is generated from the triangles in the model (mesh) that intersect with the corresponding layer height, and is represented by a polygonal chain.

The `toolpath-gen` is similarly developed on top of `t43`. During each repetition, the `toolpath-gen` picks up the diagrams with their corresponding heights from `layer-gen`, and generates nozzle toolpath (G-code) used to manufacture them.

The firmware performs the parsing of G-code generated from `toolpath-gen`. It is a collection of core functionalities provided by Klipper, including the computation of precise nozzle movement and the generation of stepper events. The stepper events are then converted to signals passed to the printer hardware. Note that the benign users are oblivious to migration from REE to TEE since it does not change the parsing results.

## 6.2. Secure Information Extraction

The extraction of information begins by scanning the surface of the fragments of the printed object (Figure 9b) with a Leica S9D microscope, which provides a high resolution that captures their rugged surface.

Due to the limitation of field of view, the microscope is unable to capture the entire fragment all at once. To address this issue, the fragment to be examined is fixed on a motorized rail slider (see Figure 10b). During the information extraction process, the fragment slides over the field of view of the microscope, which takes series of pictures in the meantime. Note that the pictures are taken so that every two consecutive pictures overlap. This feature allows us to fuse them together and obtain a picture of the entire fragment using ImageJ with the stitching plugin [57].

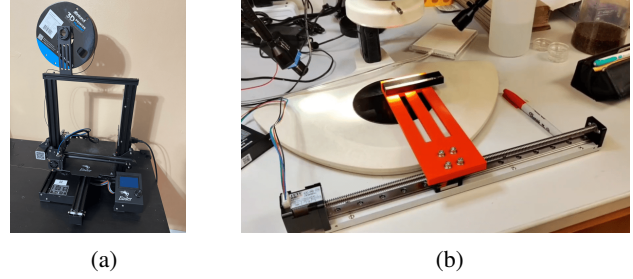


Figure 10: (a) The creality Ender 3 3D printer used in prototyping and experiments. (b) The fragment moves with the motorized slider, and the Leica S9D microscope takes a series of images of different parts of it.

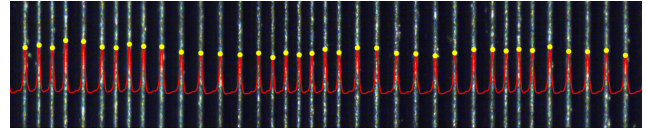


Figure 11: The reading of a fragment (cropped due to space limit), in which every bright line is the center of a layer. The pixel values (in gray scale) are accumulated and normalized for every column and displayed in red. The peaks are marked by yellow dots, which reveal the distance between every two consecutive bright lines.

In the resulting stitched image, shown in Figure 11, the bright lines are the center of each layer. To automatically read the bits from this image, we implemented `info_parser`, a program that reads the distance between every two adjacent lines, and places them in an array. Recall that there are two types of layers, the thin (0.12 mm) and the thick (0.18 mm). Hence, the elements in the array can be placed in three categories, i.e., two adjacent thin layers (thin-thin), a thin layer followed by a thick one or vice versa (thin-thick), and two adjacent thick layers (thick-thick). `info_parser` then applies  $K$ -means clustering with  $K = 3$  in order to categorize the elements.

Next, `info_parser` examines the clustering results and corrects potential errors resulting from the lighting environment during microscope reading or the image distortion in stitching. The embedding method (Figure 8) imposes certain patterns, which allow such correction. For example, a thin-thin distance must appear adjacent to another thin-thin distance, and in between thin-thin and thick-thick there must be a thin-thick.

For each layer, the program determines whether it is a thick one or a thin one by the distances from its adjacent lines, e.g., a thin line may have a thick-thick distance on its left and a thick-thin distance on its right. This concludes the reading of bits from fragments.

Finally, the bit strings that were recovered from the fragments go through the BRC decoding procedure, whose pseudo-code is given in Algorithm 2 and implementation is made in Python with `reed_solomon` codec [58], and the original information  $w$  is recovered.

## 7. Security Analysis

We provide analysis on the security of SIDE framework with respect to several potential attacks. We emphasize that the goal of the adversary is not to fail the printing process. Instead, the adversary wishes to jeopardize the flow of information embedding and extraction, without affecting the printing process of the desired crime tool.

### 7.1. Man-in-the-Middle Attack

In the scenario where the communication between the printer control board and the printer hardware is not secure, the adversary may insert themselves as a man in the middle. Specifically, the adversary hijacks the stepper events sent to the printer hardware that associate to the stepper motor which moves the nozzle along the  $z$  direction. The adversary modifies the stepper events and hence strips off the embedded bits. However, since this process moves layers to incorrect heights, it results in a discrepancy between the printed tool and the 3D model in their geometric shapes, and the tool may lose its functionality.

### 7.2. Spoofing Attack

The adversary may conduct a spoofing attack by detaching the printer hardware from the designated control board, and operating the hardware with an alternative one which does not embed bits in the printed tool. To tackle this attack (as well as the MIIM attack), the printer hardware must not print unless the control board identifies itself. Numerous methods have been developed to achieve this goal, e.g., cryptographic authentication. However, employing them is outside of the scope of this paper.

### 7.3. Denial-of-Service Attack

Since SIDE embeds information along the printing direction, the printed object must be of at least a certain height in order to hold the BRC codeword. This fact allows the adversary to conduct a denial-of-service attack on information embedding, since the 3D printer must also be available for small objects. As such, the adversary may partition the 3D models in shorter pieces and print them individually. Next, the adversary joins the pieces together with some fasteners or adhesives before committing the crime. The information embedding process is hereby bypassed.

However, we note that this process has negative impacts on the quality of the prints, since the joints are the most fragile. Indeed, the tools made by joining smaller pieces are unlikely to bear mechanically strength that is enough for criminal use. For example, a printed firearm must maintain its geometric shape after every shot under a chamber pressure, which may exceed 50,000 psi. Thus, we do not consider the printing successful, as this attack does not persevere the functionality of the printed object.

## 7.4. Information-Availability Attack

In order to jeopardize information extraction, the adversary may attempt to compromise the availability of the information that can be read from the fragments. Specifically, we consider a scenario in which the adversary prints the tool, commits the crime, and damages the tool physically in order to make the embedded bits unavailable for reading. We assume that the adversary has limited time and limited access to resources, and hence unable to damage the tool in any arbitrary fashion.

**Excessive Breaking:** As noted in the previous section, the printed tool should be mechanically rigid enough for criminal use. As a result, with human-powered equipment such as hammer or saw, the adversary must invest intensive time efforts to excessively break the tool such that the security parameter  $t$  can be exceeded. This is infeasible since the adversary has only a very limited time after committing the crime by assumption. Otherwise, the adversary may seek help from power equipment such as grinder or jigsaw, which also violates our assumption that the resources accessible by the adversary is restricted (note that household equipment, e.g., a blender, is unlikely to bear enough power to break the printed tool into fine grained pieces, even if it is printed with thermoplastic). In addition, excessive breaking (e.g., using a hammer) is likely to cause irregular breaks, i.e., which are not aligned against the printing axis. As discussed in Section 3 (see also Figure 5 and Figure 6) irregular breaks can likely be put back together using the topology of the object, leaving the de-facto number of breaks much smaller.

**Surface Altering:** We note that SIDE is inherently immune to this type of attacks by its design. Recall that SIDE embeds information by altering physical elements on the printing direction (e.g., layer thickness), which is an intrinsic property of the printed object and cannot be altered by post processings on the surface. Indeed, the reading of bits does not require the surface of the fragment to be free of adversarial tampering, as less-economical solutions, such as an industrial CT scanner, can be used to infer the layer thickness via tomographic analysis.

**Hiding:** We consider the case in which the time and accessible resource, although limited, allow the adversary to take away some small fragments from the crime scene, or equivalently, to concentrate all efforts to make bits in small intervals unreadable. For example, the adversary may pick a fragment and melt a small portion of it with a lighter. However, as long as the number of missing bits is below certain threshold, the decoding algorithm still recovers the information word  $w$  successfully, as shown in Corollary 1.

## 8. Evaluation

The evaluation of our prototype focuses on the information density (number of bits per unit distance, which is directly affected by the codeword length  $n$  of BRC) and the recoverability of data from broken objects. The former measures the amount of information that can be embedded in an

# of breaks	information length	codeword length	information rate	object length	information density
1	98 bits	243 bits	0.403	87.48 mm	1.089 bits/mm
2	120 bits	353 bits	0.340	127.08 mm	0.944 bits/mm

TABLE 1: The evaluation is conducted on two groups of five sample prints. In the first group, we embed 98 bits of information with a 1-break code, which results in codewords of 243 bits and requires the object to be at least  $\approx 87.48$ mm along the printing direction. Sample prints in the second group are resilient to 2 breaks, and the 2-break code in use has information length  $k = 120$  and codeword length  $n = 353$ . At least  $\approx 127.08$ mm along the print direction are required for the object in this case.

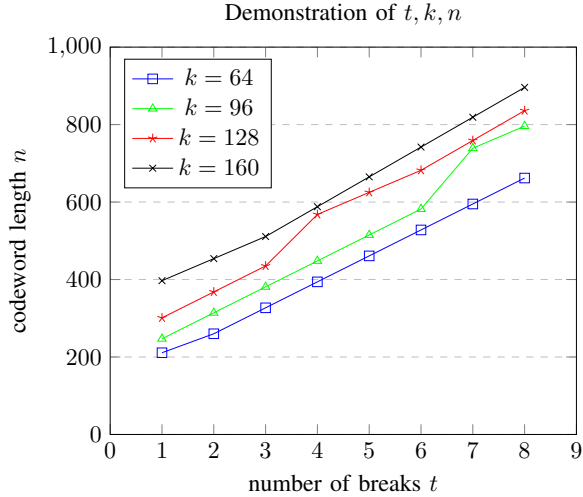


Figure 12: Demonstration of  $t, k, n$

given object, and the latter provides information extraction from broken fragments.

### 8.1. Information Density

We first analyze the codeword length  $n = |\mathbf{c}|$  provided by the BRC encoding algorithm, with respect to the security parameter  $t$  and information length  $k = |\mathbf{w}|$ . For some  $t$  and  $k$ , the length  $n$  is the number of bits required for the codeword  $\mathbf{c}$  to be break-resilient against  $t$  breaks, and is inversely related to the information density. For  $k \in \{64, 96, 128, 160\}$  and  $t \in \{1, 2, \dots, 9\}$ , the values of  $n$  is shown in Figure 12.

On the engineering side, we conduct experiments on two groups of samples, which differ in the number of embedded bits (reflected by  $k$ ) and the number of breaks that can be tolerated (reflected by  $t$ ).

For the first group, we printed five sample cuboids of dimension  $6\text{mm} \times 20\text{mm} \times 90\text{mm}$ , and implemented a 1-break code with  $k = 98$  and  $n = 243$ , which maps an information word of 98 bits to a 243 bit codeword. For each cuboid, we prepared a distinct information string and encoded it to a codeword of the aforementioned 1-break code; the codeword is embedded in the cuboid and is decodable even if broken at most once at any arbitrary location.

For the second group, we develop a 2-break code with  $k = 120$  and  $n = 353$ . The sample cuboids in

this group has a dimension of  $8\text{mm} \times 20\text{mm} \times 130\text{mm}$ . The cuboids in this group is supposed to be resilient to two breaks in any arbitrary location. Table 1 details the parameters of both groups.

### 8.2. Recoverability

We continue to evaluate the recoverability of our proposed framework. For every cuboid, we broke it apart by hand into  $t + 1$  parts, where  $t$  is the number of breaks to which it is supposedly resilient. We examined the fragments and read bits using the methods introduced in Section 6.2.

We assumed that the orientation of the fragments (i.e., the correct  $z$  direction) is known to the decoder; we postulate that closer examination of individual layers can alleviate this assumption due to the impact of gravity on the molten thermoplastic, and leave this to future work. The bit strings from the fragments were fed into the decoding algorithm, and the decoding results are compared against the original encoded data. The information extraction succeeded in all ten cases.

## 9. Conclusion

In this paper, we present SIDE, which aims to provide secure information embedding and extraction in forensic 3D fingerprinting against the malicious tampering of both 3D printers and the printed objects, in spite of the adversarial nature of this problem.

SIDE is built upon coding-theoretic techniques and hardware isolation mechanisms. On the theoretic side, we develop break-resilient codes, which is a family of codes that allow for information extraction from the printed object even if it is broken, and even if some small pieces are lost. On the engineering side, we leverage trusted execution environment to protect the integrity of the printing process, which guarantees control-flow integrity of the embedding of the break-resilient codeword. We implement a prototype of SIDE and validated our design.

We propose future studies in order to advance secure 3D fingerprinting technology further. Although our implementation and experiment are conducted in low-cost hardware, SIDE is more suitable for high-end market since incorporating a trusted execution environment in the printer significantly increases its manufacturing cost. Hence, we propose to study the integration of trusted execution environments in commodity printers. In addition, SIDE does

not include protection of the communication between the control board and the printer hardware, leaving a loophole that may be exploited to bypass secure information embedding. As such, a secure communication protocol between the two is the missing piece of the proposed framework. Moreover, the secure procurement of bits (e.g., timestamp or geolocation) for the sake of embedding from the insecure operation system is another potential research direction. On the coding-theoretical side, we propose to devise practical coding methods which operate closer to the information-theoretic limits of this model [41].

## Acknowledgment

This research was supported by the National Science Foundation under Grant CNS-2223032.

## References

- [1] M. Zhou, *3d-printed gun controversy: Everything you need to know*, accessed Sep. 15<sup>st</sup>, 2023, <https://www.cnet.com/news/politics/the-3d-printed-gun-controversy-everything-you-need-to-know/>, 2018.
- [2] H. Jiang and T. Hunt, *Untraceable ‘ghost guns’ are easier than ever to 3d print — we went inside a company that helps people do it*, accessed (Oct. 21<sup>st</sup>, 2021), <https://news.yahoo.com/untraceable-ghost-guns-easier-ever-150015562.html>, 2021.
- [3] C. M. McNulty, N. Arnas, and T. A. Campbell, “Toward the printed world: Additive manufacturing and implications for national security,” *Defense Horizons*, no. 73, p. 1, 2012.
- [4] J. Fingas, *Security firm claims to thwart iphone x’s face id with a mask*, accessed Sep. 15<sup>st</sup>, 2023, <https://www.engadget.com/2017-11-11-security-firm-claims-to-defeat-face-id-with-mask.html>, 2019.
- [5] A. Delmotte, K. Tanaka, H. Kubo, T. Funatomi, and Y. Mukaigawa, “Blind watermarking for 3-d printed objects by locally modifying layer thickness,” *IEEE Transactions on Multimedia*, vol. 22, no. 11, pp. 2780–2791, 2019.
- [6] D. Salas, D. Ebepari, M. Elverud, R. Arróyave, R. Malak, and I. Karaman, “Embedding hidden information in additively manufactured metals via magnetic property grading for traceability,” *Additive Manufacturing*, vol. 60, p. 103 261, 2022.
- [7] M. Suzuki, P. Dechrueng, S. Techavichian, P. Silapasahakornwong, H. Torii, and K. Uehira, “Embedding information into objects fabricated with 3-d printers by forming fine cavities inside them,” *Electronic Imaging*, vol. 2017, no. 7, pp. 6–9, 2017.
- [8] K. A. ElSayed, A. Dachowicz, and J. H. Panchal, “Information embedding in additive manufacturing through printing speed control,” in *Proceedings of the 2021 Workshop on Additive Manufacturing (3D Printing) Security*, 2021, pp. 31–37.
- [9] J. Voris, B. F. Christen, J. Alted, and D. W. Crawford, *Three dimensional (3d) printed objects with embedded identification (id) elements*, US Patent 9,656,428, May 2017.
- [10] J. Wee, C. I. Byatte, A. Rhoades, and D. McNeight, *Product authentication*, U.S. Patent App. 14/250,533, 2015.
- [11] J. Wee, C. I. Byatte, A. Rhoades, and D. McNeight, *Objets de vertu*, U.S. Patent App. 14/485,880, 2015.
- [12] C. Wei, Z. Sun, Y. Huang, and L. Li, “Embedding anti-counterfeiting features in metallic components via multiple material additive manufacturing,” *Additive Manufacturing*, vol. 24, pp. 1–12, 2018.
- [13] F. Chen, Y. Luo, N. G. Tsoutsos, M. Maniatakos, K. Shahin, and N. Gupta, “Embedding tracking codes in additive manufactured parts for product authentication,” *Advanced Engineering Materials*, vol. 21, no. 4, p. 1 800 495, 2019.
- [14] C. Harrison, R. Xiao, and S. Hudson, “Acoustic barcodes: Passive, durable and inexpensive notched identification tags,” in *Proceedings of the 25th annual ACM symposium on User interface software and technology*, 2012, pp. 563–568.
- [15] M. Usama and U. Yaman, “Embedding information into or onto additively manufactured parts: A review of qr codes, steganography and watermarking methods,” *Materials*, vol. 15, no. 7, p. 2596, 2022.
- [16] K. A. ElSayed, A. Dachowicz, M. J. Atallah, and J. H. Panchal, “Information embedding for secure manufacturing: Challenges and research opportunities,” *Journal of Computing and Information Science in Engineering*, vol. 23, no. 6, 2023.
- [17] Z. Li, A. S. Rathore, C. Song, S. Wei, Y. Wang, and W. Xu, “Printracker: Fingerprinting 3d printers using commodity scanners,” in *Proceedings of the 2018 ACM sigsac conference on computer and communications security*, 2018, pp. 1306–1323.
- [18] H. T. Maia, D. Li, Y. Yang, and C. Zheng, “Layer-code: Optical barcodes for 3d printed shapes,” *ACM Trans. Graph.*, vol. 38, no. 4, Jul. 2019, ISSN: 0730-0301. [Online]. Available: <https://doi.org/10.1145/3306346.3322960>.
- [19] J.-U. Hou, D.-G. Kim, S. Choi, and H.-K. Lee, “3d print-scan resilient watermarking using a histogram-based circular shift coding structure,” in *Proceedings of the 3rd ACM Workshop on Information Hiding and Multimedia Security*, ser. IH&MMSec ’15, Portland, Oregon, USA: Association for Computing Machinery, 2015, pp. 115–121, ISBN: 9781450335874. [Online]. Available: <https://doi.org/10.1145/2756601.2756607>.
- [20] K. D. D. Willis and A. D. Wilson, “Infrastructs: Fabricating information inside physical objects for imaging in the terahertz region,” *ACM Trans. Graph.*, vol. 32, no. 4, Jul. 2013, ISSN: 0730-0301. [Online]. Available: <https://doi.org/10.1145/2461912.2461936>.
- [21] D. Li, A. S. Nair, S. K. Nayar, and C. Zheng, “Air-code: Unobtrusive physical tags for digital fabrication,” in *Proceedings of the 30th Annual ACM Sym-*

- posium on User Interface Software and Technology, ser. UIST '17, Québec City, QC, Canada: Association for Computing Machinery, 2017, pp. 449–460, ISBN: 9781450349819. [Online]. Available: <https://doi.org/10.1145/3126594.3126635>.
- [22] J.-W. Cho, R. Prost, and H.-Y. Jung, “An oblivious watermarking for 3-d polygonal meshes using distribution of vertex norms,” *IEEE Transactions on Signal Processing*, vol. 55, no. 1, pp. 142–155, 2007.
- [23] OP-TEE, *Security firm claims to thwart iphone x’s face id with a mask*, <https://www.trustedfirmware.org/projects/op-tee/>, 2024.
- [24] I. Corporation, *Intel(r) software guard extensions for linux\* os*, <https://github.com/intel/linux-sgx>, 2024.
- [25] K. Krawiecka, A. Kurnikov, A. Paverd, M. Manan, and N. Asokan, “Safekeeper: Protecting web passwords using trusted execution environments,” in *Proceedings of the 2018 World Wide Web Conference*, 2018, pp. 349–358.
- [26] F. Schwarz and C. Rossow, “{Seng}, the {sgx-enforcing} network gateway: Authorizing communication from shielded clients,” in *29th USENIX Security Symposium (USENIX Security 20)*, 2020, pp. 753–770.
- [27] J. B. Djoko, J. Lange, and A. J. Lee, “Nexus: Practical and secure access control on untrusted storage platforms using client-side sgx,” in *2019 49th Annual IEEE/IFIP International Conference on Dependable Systems and Networks (DSN)*, IEEE, 2019, pp. 401–413.
- [28] A. Baumann, M. Peinado, and G. Hunt, “Shielding applications from an untrusted cloud with haven,” *ACM Transactions on Computer Systems (TOCS)*, vol. 33, no. 3, pp. 1–26, 2015.
- [29] F. Schuster, M. Costa, C. Fournet, *et al.*, “Vc3: Trustworthy data analytics in the cloud using sgx,” in *2015 IEEE Symposium on Security and Privacy*, IEEE, 2015, pp. 38–54.
- [30] R. Poddar, C. Lan, R. A. Popa, and S. Ratnasamy, “{Safebricks}: Shielding network functions in the cloud,” in *15th USENIX Symposium on Networked Systems Design and Implementation (NSDI 18)*, 2018, pp. 201–216.
- [31] T. Hunt, Z. Jia, V. Miller, *et al.*, “Telekine: Secure computing with cloud {gpus},” in *17th USENIX Symposium on Networked Systems Design and Implementation (NSDI 20)*, 2020, pp. 817–833.
- [32] F. Mo, H. Haddadi, K. Katevas, E. Marin, D. Perino, and N. Kourtellis, “Ppfl: Privacy-preserving federated learning with trusted execution environments,” in *Proceedings of the 19th annual international conference on mobile systems, applications, and services*, 2021, pp. 94–108.
- [33] F. Alder, J. Van Bulck, F. Piessens, and J. T. Mühlberg, “Aion: Enabling open systems through strong availability guarantees for enclaves,” in *Proceedings of the 2021 ACM SIGSAC Conference on Computer and Communications Security*, 2021, pp. 1357–1372.
- [34] J. Wang, A. Li, H. Li, C. Lu, and N. Zhang, “Rt-tee: Real-time system availability for cyber-physical systems using arm trustzone,” in *2022 IEEE Symposium on Security and Privacy (SP)*, IEEE, 2022, pp. 352–369.
- [35] S. Pinto, H. Araujo, D. Oliveira, J. Martins, and A. Tavares, “Virtualization on trustzone-enabled microcontrollers? voilà!” In *2019 IEEE Real-Time and Embedded Technology and Applications Symposium (RTAS)*, IEEE, 2019, pp. 293–304.
- [36] R. Roth, *Introduction to Coding Theory*. Cambridge University Press, 2006.
- [37] I. Shomorony and A. Vahid, “Communicating over the torn-paper channel,” in *IEEE Globecom*, 2020, pp. 1–6.
- [38] I. Shomorony and A. Vahid, “Torn-paper coding,” *IEEE Trans. Inf. Theory*, vol. 67, no. 12, pp. 7904–7913, 2021.
- [39] A. N. Ravi, A. Vahid, and I. Shomorony, “Capacity of the torn paper channel with lost pieces,” in *Proc. IEEE Int. Symp. Inf. Theory*, IEEE, 2021, pp. 1937–1942.
- [40] D. Bar-Lev, S. M. E. Yaakobi, and Y. Yehezkeally, “Adversarial torn-paper codes,” *IEEE Trans. Inf. Theory*, 2023.
- [41] C. Wang, J. Sima, and N. Raviv, *Break-resilient codes for forensic 3d fingerprinting*, 2023. arXiv: [2310.03897 \[cs.IT\]](https://arxiv.org/abs/2310.03897).
- [42] K. Thompson, “Reflections on trusting trust,” *Communications of the ACM*, vol. 27, no. 8, pp. 761–763, 1984.
- [43] F. Bals, *What is the xz utils backdoor : Everything you need to know about the supply chain attack*, accessed (April. 11<sup>st</sup>, 2024), <https://www.synopsys.com/blogs/software-security/xz-utils-backdoor-supply-chain-attack.html>, 2024.
- [44] M. Levy and E. Yaakobi, “Mutually uncorrelated codes for dna storage,” *IEEE Transactions on Information Theory*, vol. 65, no. 6, pp. 3671–3691, 2018.
- [45] V. Levenshtein, “Decoding automata invariant with respect to the initial state,” *Problems of Cybernetics*, vol. 12, pp. 125–136, 1964.
- [46] V. Levenshtein, “Maximum number of words in codes without overlaps,” *Problemy Peredachi Informatsii*, vol. 6, no. 4, pp. 355–357, 1970.
- [47] E. Gilbert, “Synchronization of binary messages,” *IRE Transactions on Information Theory*, vol. 6, no. 4, pp. 470–477, 1960.
- [48] D. Bajic and J. Stojanovic, “Distributed sequences and search process,” in *2004 IEEE International Conference on Communications (IEEE Cat. No.04CH37577)*, vol. 1, 2004, 514–518 Vol.1.
- [49] D. Bajic and T. Loncar-Turukalo, “A simple suboptimal construction of cross-bifix-free codes,” *Cryptography and Communications*, vol. 6, no. 1, pp. 27–36, 2013.

- [50] Y. M. Chee, H. M. Kiah, P. Purkayastha, and C. Wang, “Cross-bifix-free codes within a constant factor of optimality,” *IEEE Transactions on Information Theory*, vol. 59, no. 7, pp. 4668–4674, 2013.
- [51] S. Bilotta, E. Pergola, and R. Pinzani, “A new approach to cross-bifix-free sets,” *IEEE Transactions on Information Theory*, vol. 58, no. 6, pp. 4058–4063, 2012.
- [52] S. R. Blackburn, “Non-overlapping codes,” *IEEE Transactions on Information Theory*, vol. 61, no. 9, pp. 4890–4894, 2015.
- [53] G. Wang and Q. Wang, “Q-ary non-overlapping codes: A generating function approach,” *IEEE Transactions on Information Theory*, vol. 68, no. 8, pp. 5154–5164, 2022.
- [54] O. Elishco, R. Gabrys, E. Yaakobi, and M. Médard, “Repeat-free codes,” *IEEE Transactions on Information Theory*, vol. 67, no. 9, pp. 5749–5764, 2021.
- [55] Klipper3d, *Klipper*, <https://github.com/Klipper3d/klipper>, 2024.
- [56] L. Huang, *T43*, <https://github.com/LingDong-/t43>, 2024.
- [57] S. Preibisch, S. Saalfeld, and P. Tomancak, “Globally optimal stitching of tiled 3D microscopic image acquisitions,” *Bioinformatics*, vol. 25, no. 11, pp. 1463–1465, Apr. 2009, ISSN: 1367-4803. [Online]. Available: <https://doi.org/10.1093/bioinformatics/btp184>.
- [58] tomerfiliba-org, *Reedsolomon*, <https://github.com/tomerfiliba-org/reedsolomon>, 2024.

## Appendix A. Distinct Strings

Alg. 3 offers a procedure that maps an input word  $w \in \{0, 1\}^{l-m-1}$  to  $dStrings$ , which is an array of  $l$  pairwise distinct binary strings of length  $m$ . Besides, the inverse operation, as given in Alg. 4, outputs  $w$  given the array  $dStrings$ .

The encoding algorithm first appends a 1 to  $w$  (line 1), and as a result,  $|w| = l \cdot m$ . The word  $w$  is segmented to  $l$  intervals of length  $m$  and placed in a tentative array  $dStrings$  (line 2). The segments are not necessarily pairwise distinct at this point, and they are referred as the *original*.

The encoding algorithm continues to look for identical original segments, deletes one of them, and appends a *new* binary string to  $dStrings$ ; this new string contains the indexing information of the two identical binary strings which allows for decoding at a later point in time. Moreover, we end every new string with a 0 to distinguish it from the right most original segment which ends with a 1.

With indices  $i$  and  $i_{end}$  initially set to 0 and  $l - 1$ , the algorithm looks up every index  $j \in [i + 1, i_{end}]$  for a match, i.e.,  $dStrings[i]$  is identical to  $dStrings[j]$  (line 5). Once a match is found, the latter is deleted from  $dStrings$  (line 7) and the indices  $i, j$  are recorded in a binary string to be placed at the end of  $dStrings$ , which is responsible for the recovery of the deleted entry.

Note that, naïvely defining the new strings as the concatenation of binary representations of  $i$  and  $j$  may introduce more repeated strings; it may coincide with existing elements in  $dStrings$ . To address this issue, the algorithm starts looking for an *alternative* binary representation of  $j$  which is not identical to the first  $\lceil \log l \rceil + 1$  bits of every existing element in  $dStrings$ .

Starting from  $j' = 0$ , the following procedure is repeated  $j$  times. In each time,  $j'$  is increased by 1 (line 11). Then, it continues to increase until its binary representation in  $\lceil \log l \rceil + 1$  bits does not coincide with the first  $\lceil \log l \rceil + 1$  bits of every existing element in  $dStrings$  (line 12). One may imagine this process as looking for the  $j$ -th available parking slot in a row, in which some have been occupied (unavailable). A slot is unavailable if the binary representation of its index coincides with the first  $\lceil \log l \rceil + 1$  bits of any element in  $dStrings$ . Otherwise, it is available. Starting for index 0,  $j'$  is indeed the index of the  $j$ -th available slot.

Note that when the repetition stops,  $j'$  equals to the sum of  $j$  and the number of times the condition in line 12 was true. Recall that  $1 \leq j \leq l - 1$ , and the latter equals to the number of unavailable slots that may be encountered during the increment of  $j'$ , which is at most  $l - 1$  since there are only  $l - 1$  elements in  $dStrings$ . Therefore,  $j' \leq 2l - 2$  and can be represented by  $\lceil \log l \rceil + 1$  bits.

Therefore, we use the binary representation of  $j'$  in  $\lceil \log l \rceil + 1$  to serve as the alternative representation of  $j$ . It is concatenated with the binary representation of  $i$  (in  $\lceil \log l \rceil$  bits since  $i < l$ ) and sufficiently many 0's to make a *new* string (line 13). The new string is appended to  $dStrings$ , and is different from every other element in the first  $\lceil \log l \rceil + 1$  bits; this fact gives the following lemma.

**Lemma 4.** The new binary string being appended in line 13 is different from every existing elements in  $dStrings$ .

Lemma 4 allows us to decrease  $i_{end}$  by one (line 14) since there is no need to compare  $dStrings[j]$  with element whose index is greater than  $i_{end} - 1$ . The algorithm terminates when there is no elements of  $dStrings$  remains to be compared (line 3), and its output satisfies the following.

**Theorem 2.** Alg. 3 outputs an array  $dStrings$  of  $l$  pairwise distinct binary strings of length- $m$ .

*Proof of Theorem 2.* Assume, for sake of contradiction, that there exist  $a, b \in [0, l - 1]$  and  $a < b$  such that  $dStrings[a] = dStrings[b]$ . There are two possible cases for  $dStrings[b]$ .

If  $dStrings[b]$  is a new string constructed in line 13, then it is distinct from every other elements on its left by Lemma 4, a contradiction. If  $dStrings[b]$  is not a new string, then the  $dStrings[a]$  on its left is not as well. As such,  $dStrings[b]$  would have been deleted in line 7 when  $i = a$  and  $j = b$ , a contradiction.  $\square$

We proceed to introduce the decoding procedure in Algorithm 4, which is essentially the inverse operation of the encoding process. Given the array  $dStrings$ , the decoding



---

**Algorithm 3** D-ENCODE (distinct strings encoding)

---

**Input:** A binary string  $\mathbf{w} \in \{0, 1\}^{l \cdot m - 1}$ , where  $l, m$  are positive integers such that  $m \geq \lceil 2 \log l \rceil + 2$ .

**Output:** Array `dStrings` of  $l$  length- $m$  pairwise distinct binary strings.

```
1: Let  $\mathbf{w} \leftarrow \mathbf{w} \circ 1$ ,  $i \leftarrow 0$ ,  $i_{\text{end}} \leftarrow l - 1$ 
2: Let  $\text{dStrings}[a] \leftarrow \mathbf{w}[a \cdot m : (a + 1) \cdot m]$  for  $a \in [0, l - 1]$ .
3: while  $i < i_{\text{end}}$  do
4:    $j \leftarrow i + 1$ 
5:   while  $j \leq i_{\text{end}}$  do
6:     if  $\text{dStrings}[i] = \text{dStrings}[j]$  then
7:        $\text{dStrings} \leftarrow (\text{dStrings}[0 : j - 1], \text{dStrings}[j + 1 : l - 1])$ 
8:        $j' \leftarrow 0$ 
9:       repeat  $j$  times:
10:        do
11:           $j' \leftarrow j' + 1$ 
12:          while  $\exists r \in [l - 2]$  s.t.,  $\text{dStrings}[r - 1][0 : \lceil \log l \rceil] = \text{BINARY}(j', \lceil \log l \rceil + 1)$ 
13:             $\text{dStrings}.\text{APPEND}(\text{BINARY}(j', \lceil \log l \rceil + 1) \circ \text{BINARY}(i, \lceil \log l \rceil) \circ 0^{m - 2 \lceil \log l \rceil - 1})$ 
14:             $i_{\text{end}} \leftarrow i_{\text{end}} - 1$ 
15:          else
16:             $j \leftarrow j + 1$ 
17:         $i \leftarrow i + 1$ 
18: return dStrings
```

---

---

**Algorithm 4** D-DECODE (distinct strings decoding)

---

**Input:** Array `dStrings` of  $l$  length- $m$  pairwise distinct binary strings.

**Output:** The information word  $\mathbf{w} \in \{0, 1\}^k$  used to generate `dStrings`.

```
1: while  $\text{dStrings}[-1][-1] = 0$  do
2:    $i \leftarrow \text{INTEGER}(\text{dStrings}[l][\lceil \log l \rceil + 2 : 2 \lceil \log l \rceil + 1])$ 
3:    $j, j' \leftarrow \text{INTEGER}(\text{dStrings}[l - 1][1 : \lceil \log l \rceil + 1])$ 
4:   for all  $r \in [0, l - 2]$  and  $s \in [j' - 1]$  do
5:     if  $\text{dStrings}[r][1 : \lceil \log l \rceil + 1] = \text{BINARY}(s, \lceil \log l \rceil + 1)$  then  $j \leftarrow j - 1$ 
6:    $\text{dStrings} \leftarrow (\text{dStrings}[0 : j - 1], \text{dStrings}[i], \text{dStrings}[j : l - 2])$ 
7:  $\mathbf{w} \leftarrow \text{dStrings}[0] \circ \dots \circ \text{dStrings}[l - 1]$ 
8: return  $\mathbf{w}[-1]$ 
```

---

algorithm reads  $i, j'$  from the rightmost element if it is a constructed new string, i.e., if last bit of which is 0 (line 1). Recall that a new string is created when two identical strings is found, with  $i$  being the index of the first one (the reference) and  $j'$  being the *alternative* index of the second (the referent).

Line 2 reads the value of  $i$ , and line 3 reads the value of  $j'$ . Recall that  $j'$  is the index of the  $j$ -th available slots in a row. Hence, the variable  $j$  is initially set to  $j'$ , and then subtracted by the number of unavailable slots with indices less than  $j'$  to reaches the actual index of the referent (line 4–5). Together,  $i, j$  enable the recovery of the referent, and the rightmost element is deleted (line 6). Once all new strings have been consumed in the aforementioned process, the decoding is concluded and  $\mathbf{w}$  is returned (line 8).